EB1 regulates microtubule dynamics and tubulin sheet closure in vitro.

Benjamin Vitre, Frédéric M. Coquelle, Claire Heichette, Cyrille Garnier, Denis Chrétien, Isabelle Arnal

EB1 promotes microtubule dynamics and regulates tubulin sheet closure *in vitro.*

Benjamin Vitre[1], Frédéric M. Coquelle[1], Claire Heichette[1], Cyrille Garnier[1], Denis Chrétien[1] and Isabelle Arnal[1]

[1]Université de Rennes 1, Interactions Cellulaires et Moléculaires,
Centre Nationale de la Recherche Scientifique, Unité Mixte de Recherche 6026,
Institut Fédératif de Recherche 140, Génétique Fonctionnelle Agronomie et Santé,
Campus de Beaulieu,
263, Avenue du Général Leclerc,
35042 Rennes,
France

Correspondence should be addressed to I.A. (isabelle.arnal@univ-rennes1.fr) or D.C. (denis.chretien@univ-rennes1.fr).

End binding 1 (EB1) is a plus-end-tracking protein (+TIP) that localizes to microtubule plus ends where it modulates their dynamics and interactions with intracellular organelles[1, 2]. Although the regulating activity of EB1 on microtubule dynamics has been studied in cells[3-6] and purified systems[7-13], the molecular mechanisms involved in its specific activity are still unclear. Here, we describe how EB1 regulates the dynamics and structure of microtubules assembled from pure tubulin. We found that EB1 stimulates microtubule spontaneous nucleation and growth rate, and promotes both catastrophes (transitions from growth to shrinkage) and rescues (reverse events). Electron cryomicroscopy showed that EB1 induces the initial formation of tubulin sheets that rapidly close into the common 13-protofilament-microtubule architecture. Our results suggest that EB1 favours the lateral association of free tubulin at microtubule sheet edges, thereby stimulating nucleation, sheet growth and closure. The reduction of sheet length at microtubule growing ends, together with the elimination of stressed microtubule lattices, may account for catastrophes. Conversely, occasional binding of EB1 to the microtubule lattice may induce rescues.

Microtubules are unstable polymers that switch stochastically between growing and shrinking states, a particular behaviour known as dynamic instability[14]. Essential for this process is the tubulin-bound GTP hydrolysis that occurs during microtubule assembly, since it creates an unstable lattice that can rapidly depolymerise[14]. Microtubule growth involves the formation of outwardly curved tubulin sheets that gradually close into tubes, and which are thought to protect the lattice from catastrophe events[15, 16]. Catastrophes may arise from loss of this capping structure through occasional closure of the sheets onto energetically unfavourable configurations[17]. Conversely, rescues may involve a metastable intermediate state between disassembly and assembly[18]. Catastrophes and rescues are finely regulated in cells and can be either stimulated or inhibited depending on the cell activity[14]. Several proteins interact with unpolymerised tubulin and/or microtubules to modulate their dynamic properties[19]. Amongst them, EB1 is a highly conserved +TIP that was first described as a partner of the tumour suppressor APC[1]. EB1 accumulates at microtubule plus ends through a treadmilling process characterized by an association with the newly growing end coupled with a rapid dissociation from the lattice older part[2]. The recognition of a specific structure at microtubule plus end (e.g. the growing tubulin sheet) may be the targeting mechanism involved, rather than a copolymerisation with tubulin dimers[8, 9, 12, 20, 21]. Despite several studies concerning the role of EB1 in the regulation of microtubule dynamics, its precise effects on the dynamic instability

parameters are still controversial. For instance, in budding yeast[4] and *Drosophila* cells[3], EB1 has been reported to increase both catastrophes and rescues when, in *Xenopus* egg extracts[12] as well as in fission yeast[5], it was mentioned to inhibit catastrophes. Likewise, *in vitro* studies have shown that EB1 promotes pure tubulin polymerisation, whereas other works have suggested that this activity requires an additional factor, such as APC or $p150^{Glued}$ dynactin-component[7, 9-11, 13]. Thus, it remains unclear whether EB1 modulates microtubule dynamics on its own, and how this activity is mediated at the structural level.

We first investigated the effects of EB1 on microtubule dynamic instability using video-enhanced differential interference contrast (VE-DIC) light microscopy. Microtubules were assembled from centrosomes at 10 μM tubulin and increasing concentrations of EB1 (0.5, 1.0, 1.5 and 2.0 μM). We limited the VE-DIC analysis to this concentration range, since self-assembly appeared above 2.0 μM, suggesting that EB1 stimulates microtubule spontaneous nucleation (see below). Fig. 1a presents individual centrosome-nucleated microtubule life histories, which are representative of the characteristic behaviour of 10 μM tubulin without and with 1.0 and 1.5 μM EB1 (also illustrated in Fig. 1b). The detailed values of the dynamic instability parameters are reported in Table 1. Microtubule assembly with tubulin alone was characterized by prolonged phases of growth interrupted by rare catastrophes, as reported before[22-25]. Addition of EB1 increased the microtubule growth rate (V_g) up to two fold at a concentration of 2.0 μM, and decreased the shrinkage rate (V_s) by ~1.5 and ~2.2 fold at 1.5 and 2.0 μM EB1, respectively. This decrease in the shrinkage rate at the highest EB1 concentrations was accompanied by a marked increase in the rescue frequency from 0.512 min^{-1} for the control to 4.360 min^{-1} with 2.0 μM EB1. These results indicated that EB1 started to bind to the microtubule wall above 1.5 μM, leading to a stabilization of the microtubule lattice. These observations are consistent with previous studies localizing EB1 in a punctuate manner along microtubules[5, 8, 9, 20, 26], in addition to its preferential accumulation at microtubule ends. EB1 was also found to promote the catastrophe frequency (F_{cat}) from 0.045 min^{-1} for the control up to 0.194 min^{-1} with 1.0 μM EB1, followed by a decrease to 0.100 min^{-1} and 0.123 min^{-1} at 1.5 μM and 2.0 μM EB1, respectively. This decrease can be explained by the binding of EB1 to the microtubule lattice above 1.5 μM, which counterbalanced its catastrophe promoting activity. Yet, the catastrophe frequency remained high compared to microtubules assembled with tubulin alone at concentrations giving similar growth rates[22-25]. In conclusion, our results demonstrate that EB1 has both catastrophe and rescue promoting activities. While rescues can be easily explained by EB1 molecules bound to the microtubule

wall for EB1:tubulin ratio above ~3:20, its stimulating effect on both the growth rate and the catastrophe frequency indicates that it has distinct activities at microtubule ends.

To get insight into the molecular mechanisms underlying EB1 properties, we analysed its effect on microtubule self-assembly (Fig. 2a). Tubulin was first incubated at 15 µM, i.e. below the critical concentration needed for self-assembly[25]. While microtubules did not polymerize with tubulin alone, addition of 0.9 µM EB1 induced the formation of microtubules, confirming that it stimulated both spontaneous nucleation and assembly. Likewise, addition of 0.9 and 1.5 µM EB1 to a 45 µM tubulin solution resulted in an increase of the overall mass of microtubules assembled, and in a drastic reduction of the nucleation phase. The most remarkable effect was the presence of a turbidity overshoot that happened during the assembly phase (arrowheads), suggesting that other structures transiently formed in addition to regular microtubules. A similar overshoot has been observed in the presence of both Human EB1 and $p150^{Glued}$[10]. However, only little effects of Human EB1 alone on microtubule self-assembly could be demonstrated. It remains unclear whether this discrepancy with our results is due to differences in the EB1 construct used or in assembly conditions. Large overshoots at the end of the assembly phase have been described before, and were attributed to the presence of long sheets that scattered more light than microtubules and gradually closed into tubes[27]. We could reproduce this behaviour by assembling tubulin at 90 µM, which gave similar initial assembly kinetics than with 45 µM tubulin and 1.5 µM EB1, as determined by spectrophotometry (Fig. 2a) and VE-DIC light microscopy (data not shown). While in the former conditions, the overshoot spread over ~15 min before the assembly reached the plateau, it lasted only a few minutes in the presence of EB1 and ended up before the plateau was attained.

To investigate the structures formed during the turbidity overshoot in the presence of EB1, we used electron cryomicroscopy on samples vitrified at different assembly time points. Tubulin was polymerized at 45 µM with 1.5 µM EB1 (Fig. 2a) and samples were frozen during the elongation phase (0.5 min), around the overshoot (2 min), and at the plateau (15 min). We first analysed the structure of microtubule ends by classifying them into three types (Fig. 2b): frayed ends, blunt ends and sheets. Sheets and blunt ends were almost equally represented during the elongation phase and around the overshoot (between 41 and 49 % of the extremities, Fig. 2c), whereas blunt ends became predominant at the plateau (74.6 %). To analyse microtubule end structure in the absence of EB1, microtubules were assembled at the

same tubulin concentration (45 μM), but samples were frozen at different times since after 0.5 and 2 min incubation at 37 °C, the assembly process was still in the nucleation phase (Fig. 2a). Therefore, specimens were prepared at comparable stages to those used in the presence of EB1, i.e. in the middle of the assembly phase (10 min) and after the reaction had fully reached the plateau (40 min). In these conditions (Fig. 2d), microtubules displayed mostly blunt ends both during the elongation phase (67.9 %) and at the plateau (73.4 %). These results were consistent with the hypothesis that the turbidity overshoot observed with EB1 was due to the formation of a high proportion of sheets during initial assembly stages. In addition, the rapid fall-off of the overshoot suggested that these sheets closed rapidly into microtubules. To investigate this question, microtubules were assembled at 90 μM tubulin, conditions providing comparable initial assembly kinetics than with 45 μM tubulin and 1.5 μM EB1, and samples were prepared at the same assembly times. In these conditions (Fig. 2e), microtubules displayed a higher proportion of sheets during the elongation phase (83.2 % at 0.5 min), which decreased at the overshoot (57.6 % at 2 min) to reach values comparable to the two preceding ones at the plateau (20.1 % at 15 min). Hence, these data show that EB1 induces the formation of a lower proportion of sheets compared to microtubules assembled with tubulin alone and similar assembly kinetics. The sheet length distributions revealed the same trends as those observed for the sheet proportions (Supplementary Information, Fig. S1): sheets were on the average shorter with tubulin alone at 45 μM than in the presence of EB1, whereas assembly of 90 μM tubulin resulted in the formation of longer sheets at the same assembly stages (Fig. 2f-h). Altogether, these results show that the turbidity overshoot observed in the presence of EB1 is due to an initial stimulation of sheet growth, followed by their rapid closure into microtubules. To confirm this observation, tubulin was polymerized with GMPCPP and DMSO, which induce the formation of unclosed microtubules[9] (Supplementary Information, Fig. S2). While in this condition, sheets were predominant (62.2 %), assembly in the presence of EB1 resulted in the formation of a majority of closed microtubules (75.5 %), demonstrating that, like its yeast-orthologue Mal3p[9], EB1 has a sheet closure promoting activity.

It has been proposed that catastrophes are a consequence of occasional closure of the growing sheets onto unfavourable configurations[17]. Since EB1 promoted catastrophes (Table 1), we wondered whether it would affect microtubule lattice structure. Microtubule protofilament number can be determined on electron cryomicroscope images by looking at their fringe patterns[28] (Fig. 3a). Microtubules with 13 protofilaments arranged according to 3-start helical

families are the most energetically favourable configurations, since their protofilaments run parallel to the microtubule wall[17] (unskewed microtubule). All other protofilament and/or helix start number configurations require skewing of protofilaments and changes in the lateral curvature of the microtubule wall, processes that induce strains in the lattice[17] (skewed microtubules). Furthermore, during sheet closure, microtubules occasionally switch from one type of lattice to another (see, for example, the 12 to 13 protofilament number transition in Fig. 3a), inducing local defects in the microtubule wall[29]. Microtubule populations were determined without and with EB1 for the three conditions studied (detailed in Supplementary Information, Table S1). At 45 μM tubulin, unskewed 13-protofilament microtubules represented ~75 % of the population during elongation and at the plateau (Fig. 3b). Yet, the transition frequency (Fig. 3c) was two fold higher during elongation (F_{trans} = 0.032 μm^{-1}) than at steady state (F_{trans} = 0.015 μm^{-1}). Assembly at 90 μM provided almost the same proportion of unskewed 13-protofilament microtubules, but with a much higher transition frequency than at 45 μM tubulin. Similarly, the transition frequency decreased over time, from 0.149 μm^{-1} during elongation to 0.050 μm^{-1} at the plateau. Despite their similar elongation rate compared to microtubules polymerized at 90 μM tubulin, microtubules assembled at 45 μM tubulin with 1.5 μM EB1 were essentially composed of unskewed 13-protofilament microtubules with a much lower level of transitions. As observed for the two other conditions, the transition frequency decreased as the microtubules reached steady state conditions. These results show that EB1 favours the formation of unskewed 13-protofilament microtubules while eliminating lattice-defects that otherwise would have been incorporated in the microtubule lattice at comparable assembly kinetics. Since these experiments were performed at a lower EB1:tubulin ratio (1:30) than those used for VE-DIC light microscopy where EB1 started to bind to the microtubule lattice (above ~3:20), it seems unlikely that EB1 imposes a fixed lateral curvature between adjacent tubulin dimers to favour 13-protofilament microtubules, as proposed for the neuronal MAP (Microtubule-Associated Protein) doublecortin[30]. Our results rather suggest that, during tube closure, EB1 selects unskewed 13-protofilament microtubules by discarding stressed lattices through catastrophe events, in agreement with the mechanical-stress induced mechanism of catastrophes proposed previously[17]. The fact that EB1 stimulates catastrophes while promoting the formation of 13-protofilament microtubules and decreasing lattice-defect frequency fits with this hypothesis. However, the detailed molecular mechanism on how EB1 mediates this effect remains to be elucidated.

Microtubules assembly involves the formation of outwardly curved tubulin sheets that gradually close into tubes[24]. This outward curvature results from a balance between the intrinsic longitudinal curvature of the protofilaments that pull them out from the tube axis, and the lateral one induced by their lateral association that favours tube closure[31]. As a consequence, sheet growth and closure are intimately linked and any factor stimulating the lateral association of incoming tubulin dimers promotes tube closure. Thus, our results fit with the hypothesis that EB1 favours the interaction of tubulin dimers and/or oligomers with free lateral sites exposed at the sheet edges (Fig. 4a), a mechanism consistent with Mal3p localisation at the tube closure junction[9]. This single lattice-based effect stimulates the formation and growth of sheets, which accounts for the EB1-promoting activity on both nucleation and growth rate. The subsequent increase of the lateral curvature of sheets favours their natural closure into tubes (Fig. 4b-c), leading to a size reduction of the capping structures thought to protect microtubules from depolymerisation[15] (Fig. 4d). This implies that, although microtubules grow faster in the presence of EB1, they are also more prone to undergo catastrophes (Fig. 4e). How EB1 induces these depolymerising events remains uncertain. Nevertheless, our results suggest that EB1 eliminates stressed lattices during tube closure, leading to the preferential accumulation of unskewed 13-protofilament microtubules[17]. Such a "proofreading" mechanism might be at play in cells to impose the common unskewed 13-protofilament structure of microtubules[32]. Finally, occasional binding of EB1 to the microtubule lattice may promote rescues by strengthening protofilament lateral interactions (Fig. 4f).

Our work reveals that a +TIP is able to have both catastrophe- and rescue-promoting intrinsic activities. We propose a mechanism in which a fine regulation of the tubulin sheet formation, growth and closure accounts for the specific activity of EB1. One consequence of this mechanism is that EB1 localizes preferentially to microtubule ends, where the tubulin lateral free sites are available. Further structural studies will be needed to characterize at the molecular level the precise localisation of EB1 on microtubules. The EB1-mediated increase of microtubule growth, catastrophes and rescues, is consistent with its promoting role on microtubule dynamics observed in different cell types[3, 4]. It remains to be determined how this activity is regulated by other factors to specifically modulate catastrophe and rescue events during the cell cycle.

Methods

Protein purification

Tubulin was purified from pig brain by two assembly-disassembly cycles followed by a phosphocellulose chromatography as described before[33], and stored in BRB80 buffer (80 mM Pipes, 1 mM $MgCl_2$, 1 mM EGTA, pH 6.8) at -80 °C. Mouse EB1 cDNA (subcloned in the pET28a(+) vector) was kindly provided by Dr. N. Galjart (Erasmus University, Rotterdam, The Netherlands). Recombinant mouse EB1 with a 6-histidine tag was purified from *Escherichia coli* BL21 (Invitrogen, Cergy Pontoise, France) following the same procedure used for the purification of the H2-fragment of CLIP-170[25]. The protein was dialyzed against BRB80, centrifuged at 230,000 g for 10 min at 4 °C, frozen in liquid nitrogen, and stored at -80 °C. All protein concentrations were measured using a Biorad assay (Sigma, Lyon, France) with Bovine Serum Albumin as a standard. All reagents were from Sigma (Lyon, France).

Microtubule self assembly

Tubulin was prepared at 15, 45 and 90 μM with 1 mM GTP in BRB80 and kept 5 minutes at 4 °C before assembly. Tubulin polymerisation was induced by incubating the specimen at 36 °C, and monitored turbidimetrically at 350 nm using an UVIKON XS spectrophotometer (BIOTEK Instruments, VT, USA). In order to test EB1 activity, increasing concentrations of the recombinant protein were added to 15 or 45 μM tubulin, and were incubated 5 min at 4 °C before polymerisation. For each experiment, the temperature was shifted to 4 °C after 50-60 min recording, in order to make sure that the increase of turbidity was due to microtubule assembly and not to protein aggregation.

Video-microscopy and data analysis

Microtubules were assembled from purified centrosomes at 10 μM tubulin and increasing concentrations of EB1 (0.5, 1.0, 1.5 and 2.0 μM). Samples were prepared in perfusion chambers and observed at 36 °C with an Olympus BX-51 microscope (Rungis, France) equipped with DIC (Differential Interference Contrast) prisms and a video camera coupled to an Argus 20 image processor (Hamamatsu, Massy, France), as described before[25]. Images were recorded every 2 seconds for periods of ~ 5 min. The total recording time did not exceed 60 min for each chamber. Microtubule dynamics measurements and data analysis were carried out using NIH-Image (National Institute of Health, MD, USA) and Kaleidagraph (4^{th} version,

Synergy Software, PA, USA) softwares as described before[24]. Differences between experiments were evaluated by an unpaired *t-test* and $p<0.05$ was considered significant.

Electron cryomicroscopy

Vitreous-ice embedded samples were prepared under controlled temperature and humidity conditions[29]. For polymerisation times less than 3 min, samples were directly incubated on holey-carbon grids. For longer times, they were incubated into a tube, and put on the grid using pre-warmed tips. Specimens were observed with a FEI Tecnai G^2 Sphera electron microscope operating at 200 kV (Eindhoven, The Netherlands), equipped with a Gatan stage pre-cooled with liquid nitrogen (Gatan-France, Grandchamp, France). Images were recorded on Kodak electron image films SO-163 (Kodak-Pathé, Paris, France) under low electron dose conditions, at magnifications between 25,000 and 29,000 X and ~3 µm underfocus.

Image analysis

Negatives were digitized using a NIKON Super CoolScan 9000 ED scanner at 2540 dpi (NIKON-France, Champigny sur Marne, France). Microtubule protofilament numbers and end structures were analyzed directly on printed images. Based on their specific moiré patterns, microtubules were classified according to their protofilament numbers as described previously[28]. Microtubule length was measured with an electronic ruler (Run-Mate, Metland, France), and was used to determine the percentage of each microtubule category. Microtubule extremities were classified into three different types: frayed ends, blunt ends (protofilament protrusions with a length shorter than ~12 nm) and sheets. Blunt ends were included in the sheet length measurements (Supplementary Information, Fig. S1), since they represent short extensions not visible at the resolution of the electron microscope[24]. Their size was fixed to 12 nm, which corresponds to the minimum size of the protofilament protrusion expected for a monomer 3-start helical microtubule end. Filtered images were obtained by selecting the J_0 and J_N layer-lines in the Fourier transform of straightened microtubule images, using the "Straighten Curved Objects" plugin[34] of Image J (National Institute of Health, MD, USA).

Acknowledgments

We are very grateful to Niels Galjart for providing us with the mouse EB1 construct. We thank Didier Job, Fabrice Senger, Daniel Thomas and Odile Valiron for helpful discussions, and Jean-Paul Rolland for his technical assistance with electron microscopy. This work was supported by grants from the Centre National de la Recherche Scientifique (CNRS), the Ministère de l'Enseignement Supérieur et de la Recherche (MESR) and Rennes Métropole. BV was supported by a pre-doctoral fellowship from the MESR and FMC was supported by a post-doctoral fellowship from the CNRS.

References

1. Morrison, E. E. Action and interactions at microtubule ends. *Cell. Mol. Life Sci.* **64**, 307-317 (2007).
2. Schuyler, S. C. & Pellman, D. Microtubule "plus-end-tracking proteins". the end is just the beginning. *Cell* **105**, 421-424. (2001).
3. Rogers, S. L., Rogers, G. C., Sharp, D. J. & Vale, R. D. Drosophila EB1 is important for proper assembly, dynamics, and positioning of the mitotic spindle. *J. Cell Biol.* **158**, 873-884. (2002).
4. Tirnauer, J. S., O'Toole, E., Berrueta, L., Bierer, B. E. & Pellman, D. Yeast Bim1p promotes the G1-specific dynamics of microtubules. *J. Cell Biol.* **145**, 993-1007 (1999).
5. Busch, K. E. & Brunner, D. The microtubule plus end-tracking proteins mal3p and tip1p cooperate for cell-end targeting of interphase microtubules. *Curr. Biol.* **14**, 548-559 (2004).
6. Green, R. A., Wollman, R. & Kaplan, K. B. APC and EB1 function together in mitosis to regulate spindle dynamics and chromosome alignment. *Mol. Biol. Cell* **16**, 4609-4622 (2005).
7. Manna, T., Honnappa, S., Steinmetz, M. O. & Wilson, L. Suppression of Microtubule Dynamic Instability by the +TIP Protein EB1 and Its Modulation by the CAP-Gly Domain of p150(Glued). *Biochemistry* **47**, 779-786 (2008).
8. Bieling, P. *et al.* Reconstitution of a microtubule plus-end tracking system in vitro. *Nature* **450**, 1100-1105 (2007).
9. Sandblad, L. *et al.* The Schizosaccharomyces pombe EB1 Homolog Mal3p Binds and Stabilizes the Microtubule Lattice Seam. *Cell* **127**, 1415-1424 (2006).
10. Ligon, L. A., Shelly, S. S., Tokito, M. & Holzbaur, E. L. The microtubule plus-end proteins EB1 and dynactin have differential effects on microtubule polymerization. *Mol. Biol. Cell* **14**, 1405-1417 (2003).
11. Hayashi, I., Wilde, A., Mal, T. K. & Ikura, M. Structural basis for the activation of microtubule assembly by the EB1 and p150Glued complex. *Mol. Cell* **19**, 449-460 (2005).
12. Tirnauer, J. S., Grego, S., Salmon, E. D. & Mitchison, T. J. EB1-microtubule interactions in Xenopus egg extracts: role of EB1 in microtubule stabilization and mechanisms of targeting to microtubules. *Mol. Biol. Cell* **13**, 3614-3626 (2002).
13. Nakamura, M., Zhou, X. Z. & Lu, K. P. Critical role for the EB1 and APC interaction in the regulation of microtubule polymerization. *Curr. Biol.* **11**, 1062-1067. (2001).
14. Desai, A. & Mitchison, T. J. Microtubule polymerization dynamics. *Annu. Rev. Cell Dev. Biol.* **13**, 83-117 (1997).
15. Chrétien, D., Jánosi, I., Taveau, J. C. & Flyvbjerg, H. Microtubule's conformational cap. *Cell Struct. Funct.* **24**, 299-303 (1999).
16. Mahadevan, L. & Mitchison, T. J. Cell biology: powerful curves. *Nature* **435**, 895-897 (2005).
17. Hunyadi, V., Chrétien, D. & Jánosi, I. M. Mechanical stress induced mechanism of microtubule catastrophes. *J. Mol. Biol.* **348**, 927-938 (2005).
18. Jánosi, I. M., Chrétien, D. & Flyvbjerg, H. Structural microtubule cap: stability, catastrophe, rescue, and third state. *Biophys. J.* **83**, 1317-1330 (2002).
19. Amos, L. A. & Schlieper, D. Microtubules and maps. *Adv. Protein Chem.* **71**, 257-298 (2005).

20. Ligon, L. A., Shelly, S. S., Tokito, M. K. & Holzbaur, E. L. Microtubule binding proteins CLIP-170, EB1, and p150Glued form distinct plus-end complexes. *FEBS Lett.* **580**, 1327-1332 (2006).
21. Slep, K. C. & Vale, R. D. Structural Basis of Microtubule Plus End Tracking by XMAP215, CLIP-170, and EB1. *Mol. Cell* **27**, 976-991 (2007).
22. Walker, R. A. *et al.* Dynamic instability of individual microtubules analyzed by video light microscopy: rate constants and transition frequencies. *J. Cell Biol.* **107**, 1437-1448. (1988).
23. Drechsel, D. N., Hyman, A. A., Cobb, M. H. & Kirschner, M. W. Modulation of the dynamic instability of tubulin assembly by the microtubule-associated protein tau. *Mol. Biol. Cell* **3**, 1141-1154. (1992).
24. Chrétien, D., Fuller, S. D. & Karsenti, E. Structure of growing microtubule ends: two-dimensional sheets close into tubes at variable rates. *J. Cell Biol.* **129**, 1311-1328. (1995).
25. Arnal, I., Heichette, C., Diamantopoulos, G. S. & Chretien, D. CLIP-170/tubulin-curved oligomers coassemble at microtubule ends and promote rescues. *Curr. Biol.* **14**, 2086-2095 (2004).
26. Morrison, E. E., Wardleworth, B. N., Askham, J. M., Markham, A. F. & Meredith, D. M. EB1, a protein which interacts with the APC tumour suppressor, is associated with the microtubule cytoskeleton throughout the cell cycle. *Oncogene* **17**, 3471-3477 (1998).
27. Detrich, H. W., 3rd, Jordan, M. A., Wilson, L. & Williams, R. C., Jr. Mechanism of microtubule assembly. Changes in polymer structure and organization during assembly of sea urchin egg tubulin. *J. Biol. Chem.* **260**, 9479-9490 (1985).
28. Wade, R. H., Chrétien, D. & Job, D. Characterization of microtubule protofilament numbers. How does the surface lattice accommodate? *J. Mol. Biol.* **212**, 775-786 (1990).
29. Chrétien, D., Metoz, F., Verde, F., Karsenti, E. & Wade, R. H. Lattice defects in microtubules: protofilament numbers vary within individual microtubules. *J. Cell Biol.* **117**, 1031-1040 (1992).
30. Moores, C. A. *et al.* Mechanism of microtubule stabilization by doublecortin. *Mol. Cell* **14**, 833-839 (2004).
31. Jánosi, I. M., Chrétien, D. & Flyvbjerg, H. Modeling elastic properties of microtubule tips and walls. *Eur. Biophys. J.* **27**, 501-513 (1998).
32. Tilney, L. G. *et al.* Microtubules: evidence for 13 protofilaments. *J. Cell Biol.* **59**, 267-275 (1973).
33. Ashford, A. J., Andersen, S. S. & Hyman, A. A. Preparation of tubulin from bovine brain. *Cell Biology: A Laboratory Handbook*, **Vol. 2**, 2nd edition, 205-212 (Julio E. Celis, Academic Press, San Diego, California, USA, 1998).
34. Kocsis, E., Trus, B. L., Steer, C. J., Bisher, M. E. & Steven, A. C. Image averaging of flexible fibrous macromolecules: the clathrin triskelion has an elastic proximal segment. *J. Struct. Biol.* **107**, 6-14 (1991).
35. Chrétien, D. & Fuller, S. D. Microtubules switch occasionally into unfavorable configurations during elongation. *J. Mol. Biol.* **298**, 663-676 (2000).

Table

Table 1. EB1 promotes microtubule dynamics.

Dynamical parameters were determined by VE-DIC light microscopy for microtubules assembled from purified centrosomes in the presence of 10 μM tubulin and increasing concentrations of EB1. Standard deviations are given in parentheses. The total growth and shrinkage times analyzed, as well as the number of microtubules used for each conditions, are given in the last three rows. (n) represents the total number of measurements for the growth and shrinkage rates, and the total number of observed events for the catastrophe and rescue frequencies. Catastrophe and rescue frequencies were calculated by dividing the total number of events by the time spent in growth and shrinkage, respectively. V_g, growth rate; V_s, shrinkage rate; F_{cat}, catastrophe frequency; F_{res}, rescue frequency; MT, microtubule.

Figure legends

Figure 1. EB1 stimulates catastrophes and rescues.

(a) Life histories of microtubules assembled from purified centrosomes at 10 μM tubulin in the absence (control) and in the presence of EB1 at 1.0 and 1.5 μM. Catastrophes and rescues are marked by stars and triangles, respectively. (b) Fate of a single microtubule observed at 10 μM tubulin and 1.5 μM EB1 by VE-DIC light microscopy. Arrowheads track the microtubule extremity. A catastrophe is observed at t=24 sec, and a rescue at t=30 sec. Scale bar, 1 μm.

Figure 2. EB1 stimulates microtubule self-assembly, and promotes sheet formation and closure.

(a) Effect of EB1 at different tubulin concentrations. Microtubule assembly was monitored by measuring the variations in absorbance at 350 nm. Each curve is representative of three independent experiments. Arrowheads indicate the turbidity overshoots that occur during the assembly phases in the presence of EB1. (b) Detailed views of microtubule ends observed by electron cryomicroscopy. F, frayed end (curled protofilaments), B, blunt end (protrusions shorter than ~12 nm) and S, sheet (outwardly curved extensions). Inset patterns represent the external border of the microtubule images. Scale bar, 25 nm. (c), (d) and (e) Percentages of microtubule end structures determined at different assembly times for 45 μM tubulin with 1.5 μM EB1 (c), 45 μM tubulin (d) and 90 μM tubulin (e). The number of extremities characterised was: 303 (elongation), 161 (overshoot) and 193 (plateau) for 45 μM tubulin with EB1; 106 (elongation) and 203 (plateau) for 45 μM tubulin; 309 (elongation), 290 (overshoot) and 263 (plateau) for 90 μM tubulin. (f), (g) and (h) Average sheet lengths determined at different assembly times for 45 μM tubulin with 1.5 μM EB1 (f), 45 μM tubulin (g) and 90 μM tubulin (h). For each condition, the repartition of sheet lengths showed an inverse exponential distribution as described before[24] (see Supplementary Information, Figure S1). Results include a total of 60 negatives in the presence of EB1 (20 for elongation, 18 for the overshoot and 22 for the plateau), 35 negatives for 45 μM tubulin (16 for elongation, 19 for the plateau), and 48 negatives for 90 μM tubulin (20 for elongation, 14 for the overshoot and 14 for the plateau). El., elongation; Ov., overshoot; Pl., plateau; L_{avg}, average sheet length.

Figure 3. EB1 favours unskewed 13-protofilament microtubules while eliminating lattice defects.

(a) Images of the different microtubule types observed by electron cryomicroscopy. Microtubules were classified in two main categories: microtubules with unskewed protofilaments (13 protofilaments with 3-start helices), and microtubules with skewed protofilaments (12-, 13(s)-, 14- and 15-protofilament microtubules). The 13(s) microtubules are arranged according to 2- or 4-start helices[35]. The lower micrograph shows a transition (double arrow) from 12- to 13-protofilaments within a same microtubule. Filtered versions of the images enhancing their fringe pattern are presented below each microtubule. These fringes result from the superposition of the protofilaments in the two-dimensional projection of the electron cryomicroscope image. Microtubules with unskewed 13-protofilaments display two internal fringes running parallel to the microtubule longitudinal axis over long distances. Microtubules with skewed protofilaments show alternating fringe patterns whose periodicities are related to their protofilament skew angle[28]. Scale bar, 25 nm. (b) and (c) Percentage of unskewed 13-protofilament microtubules (b) and transition frequencies (c) at different assembly stages for the three conditions studied. Freezing times are as indicated in Fig. 2c-e. With 45 μM tubulin, the total length of microtubule segments measured was about 345 μm (n=298) and 516 μm (n=436) during elongation and at the plateau, respectively. With 90 μM tubulin, the total length of microtubule segments measured was about 696 μM (n=476), 1018 μm (n=584) and 829 μm (n=478) during elongation, around the overshoot and at the plateau, respectively. In the presence of EB1, the total length of microtubule segments measured was about 673 μm (n=639), 638 μm (n=615) and 1036 μm (n=704) during elongation, around the overshoot and at the plateau, respectively. Measurements were done on the same negatives as those used for the microtubule-end structure analysis. El., elongation; Ov., overshoot; Pl., plateau.

Figure 4. Model for EB1 activity on microtubule assembly and dynamics.

We propose that EB1 (green dots) binds preferentially to the free lateral sites on protofilaments (a), where it facilitates the incorporation of incoming tubulin dimers into the tubulin lattice (blue arrows). This effect stimulates the formation and growth of sheets (b), thereby promoting both nucleation and growth rate. The subsequent increase of the lateral curvature of the sheets leads to their natural closure into tubes (b and c, red arrows). The resulting decrease in sheet length (d) makes microtubules more prone to undergo catastrophe events (e). In addition, during tube closure, EB1 may induce catastrophes by eliminating

stressed lattices (see the text for details). At higher concentration, EB1 is no longer restricted to microtubule ends, but also interacts with the microtubule wall. The subsequent reinforcement of tubulin lateral interactions promotes rescues events (f).

Table 1. EB1 promotes microtubule dynamics.

EB1 (µM)	0	0.5	1.0	1.5	2.0
V_g (µm.min $^{-1}$)	1.34 (0.47) n = 824	1.42 (0.42) n = 1421	1.95 (0.60) n = 1292	2.43 (0.51) n = 1777	2.68 (0.70) n = 496
V_s (µm.min $^{-1}$)	- 22.84 (9.34) n = 101	- 20.60 (11.64) n = 208	- 19.78 (9.35) n = 337	- 15.66 (7.72) n = 288	- 10.40 (6.28) n = 53
F_{cat} (min $^{-1}$)	0.045 n = 9	0.038 n = 16	0.194 n = 58	0.100 n = 34	0.123 n = 9
F_{res} (min $^{-1}$)	0.512 n = 3	0.301 n = 4	0.158 n = 3	2.030 n = 26	4.360 n = 8
Growth time (min)	200.00	421.05	298.97	340.00	73.17
Shrinkage time (min)	5.86	13.29	18.98	12.81	1.83
MT number	69	121	143	122	30

Table 1. EB1 promotes microtubule dynamics.
Dynamical parameters were determined by VE-DIC light microscopy for microtubules assembled from purified centrosomes in the presence of 10 µM tubulin and increasing concentrations of EB1. Standard deviations are given in parentheses. The total growth and shrinkage times analyzed, as well as the number of microtubules used for each conditions, are given in the last three rows. (n) represents the total number of measurements for the growth and shrinkage rates, and the total number of observed events for the catastrophe and rescue frequencies. Catastrophe and rescue frequencies were calculated by dividing the total number of events by the time spent in growth and shrinkage, respectively. V_g , growth rate; V_s , shrinkage rate; F_{cat} , catastrophe frequency; F_{res}, rescue frequency; MT, microtubule.

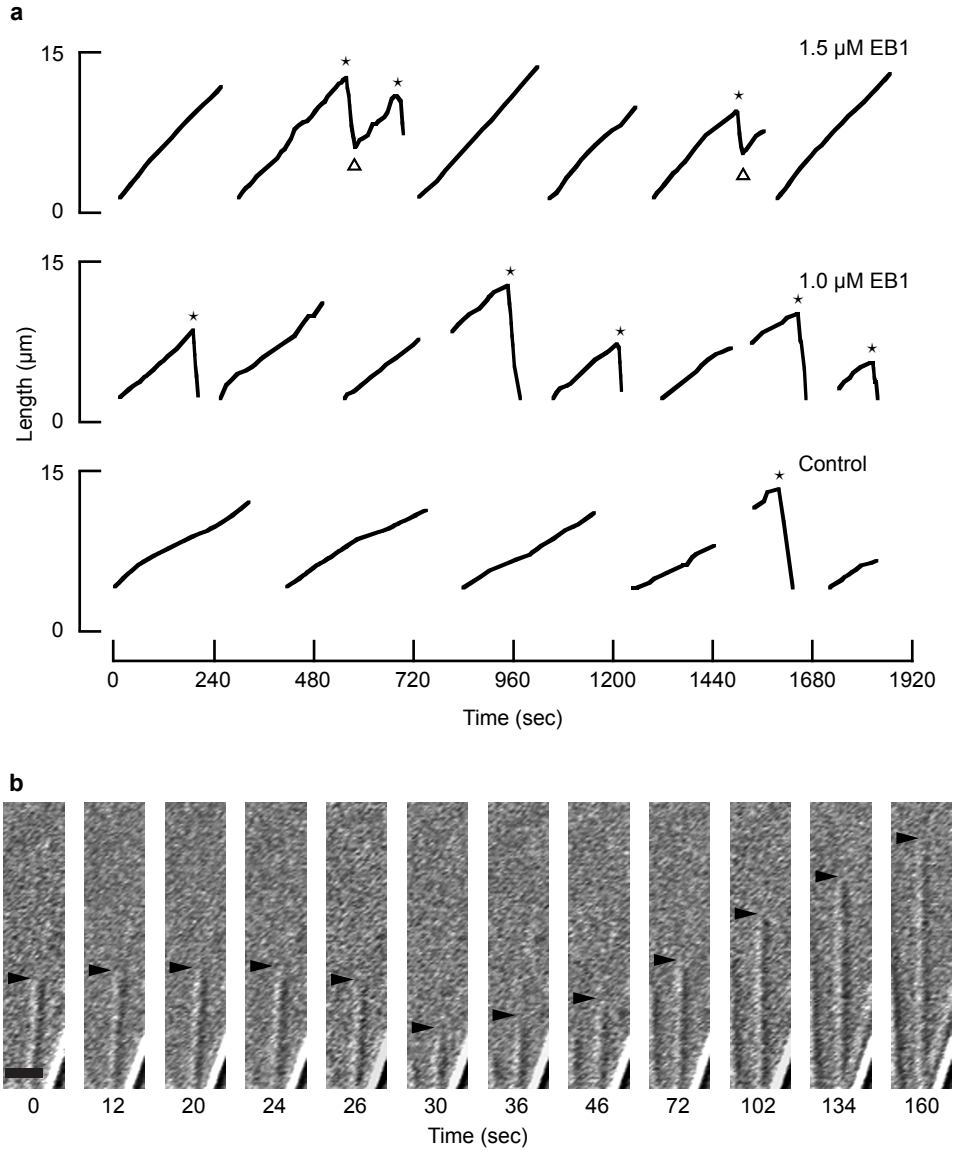

Figure 1. EB1 stimulates catastrophes and rescues.
(a) Life histories of microtubules assembled from purified centrosomes at 10 μM tubulin in the absence (control) and in the presence of EB1 at 1.0 and 1.5 μM. Catastrophes and rescues are marked by stars and triangles, respectively. (b) Fate of a single microtubule observed at 10 μM tubulin and 1.5 μM EB1 by VE-DIC light microscopy. Arrowheads track the microtubule extremity. A catastrophe is observed at t=24 sec, and a rescue at t=30 sec. Scale bar, 1 μm.

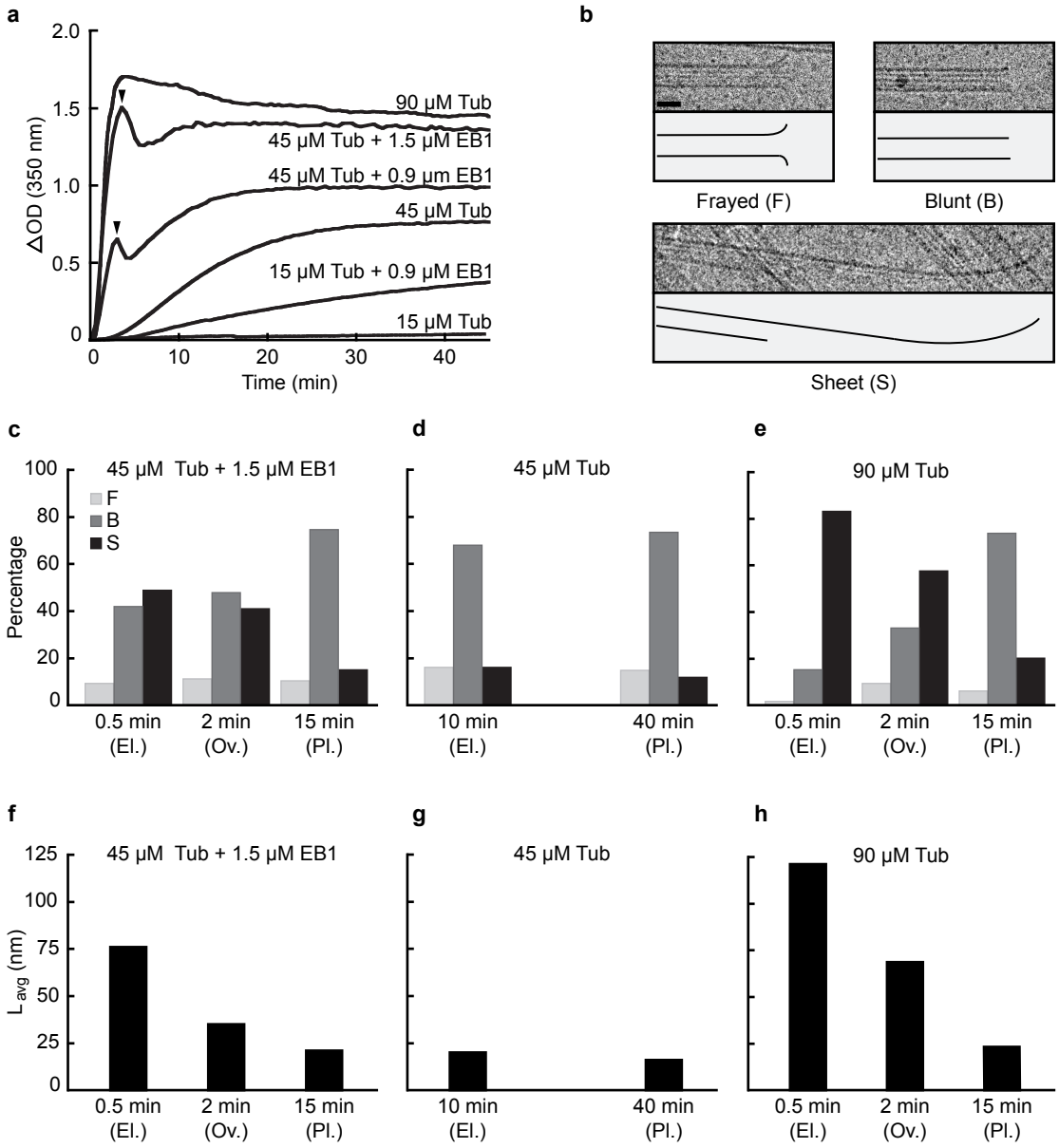

Figure 2. EB1 stimulates microtubule self-assembly, and promotes sheet formation and closure.
(a) Effect of EB1 at different tubulin concentrations. Microtubule assembly was monitored by measuring the variations in absorbance at 350 nm. Each curve is representative of three independent experiments. Arrowheads indicate the turbidity overshoots that occur during the assembly phases in the presence of EB1. (b) Detailed views of microtubule ends observed by electron cryomicroscopy. F, frayed end (curled protofilaments), B, blunt end (protrusions shorter than ~12 nm) and S, sheet (outwardly curved extensions). Inset patterns represent the external border of the microtubule images. Scale bar, 25 nm. (c), (d) and (e) Percentages of microtubule end structures determined at different assembly times for 45 µM tubulin with 1.5 µM EB1 (c), 45 µM tubulin (d) and 90 µM tubulin (e). The number of extremities characterised was: 303 (elongation), 161 (overshoot) and 193 (plateau) for 45 µM tubulin with EB1; 106 (elongation) and 203 (plateau) for 45 µM tubulin; 309 (elongation), 290 (overshoot) and 263 (plateau) for 90 µM tubulin. (f), (g) and (h) Average sheet lengths determined at different assembly times for 45 µM tubulin with 1.5 µM EB1 (f), 45 µM tubulin (g) and 90 µM tubulin (h). For each condition, the repartition of sheet lengths showed an inverse exponential distribution as described before[24] (see Supplementary Information, Figure S1). Results include a total of 60 negatives in the presence of EB1 (20 for elongation, 18 for the overshoot and 22 for the plateau), 35 negatives for 45 µM tubulin (16 for elongation, 19 for the plateau), and 48 negatives for 90 µM tubulin (20 for elongation, 14 for the overshoot and 14 for the plateau). El., elongation; Ov., overshoot; Pl., plateau; L_{avg}, average sheet length.

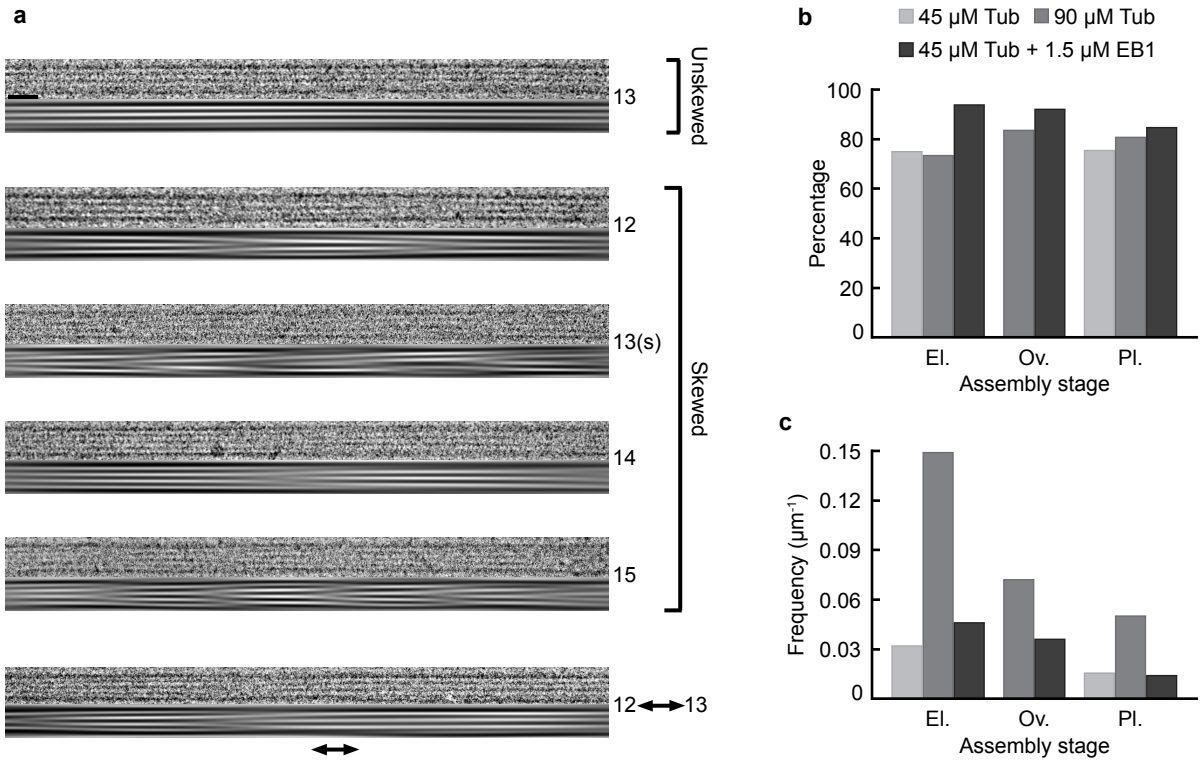

Figure 3. EB1 favours unskewed 13-protofilament microtubules while eliminating lattice defects.
(a) Images of the different microtubule types observed by electron cryomicroscopy. Microtubules were classified in two main categories: microtubules with unskewed protofilaments (13 protofilaments with 3-start helices), and microtubules with skewed protofilaments (12-, 13(s)-, 14- and 15-protofilament microtubules). The 13(s) microtubules are arranged according to 2- or 4-start helices[35]. The lower micrograph shows a transition (double arrow) from 12- to 13-protofilaments within a same microtubule. Filtered versions of the images enhancing their fringe pattern are presented below each microtubule. These fringes result from the superposition of the protofilaments in the two-dimensional projection of the electron cryomicroscope image. Microtubules with unskewed 13-protofilaments display two internal fringes running parallel to the microtubule longitudinal axis over long distances. Microtubules with skewed protofilaments show alternating fringe patterns whose periodicities are related to their protofilament skew angle[28]. Scale bar, 25 nm. (b) and (c) Percentage of unskewed 13-protofilament microtubules (b) and transition frequencies (c) at different assembly stages for the three conditions studied. Freezing times are as indicated in Fig. 2c-e. With 45 µM tubulin, the total length of microtubule segments measured was about 345 µm (n=298) and 516 µm (n=436) during elongation and at the plateau, respectively. With 90 µM tubulin, the total length of microtubule segments measured was about 696 µM (n=476), 1018 µm (n=584) and 829 µm (n=478) during elongation, around the overshoot and at the plateau, respectively. In the presence of EB1, the total length of microtubule segments measured was about 673 µm (n=639), 638 µm (n=615) and 1036 µm (n=704) during elongation, around the overshoot and at the plateau, respectively. Measurements were done on the same negatives as those used for the microtubule-end structure analysis. El., elongation; Ov., overshoot; Pl., plateau.

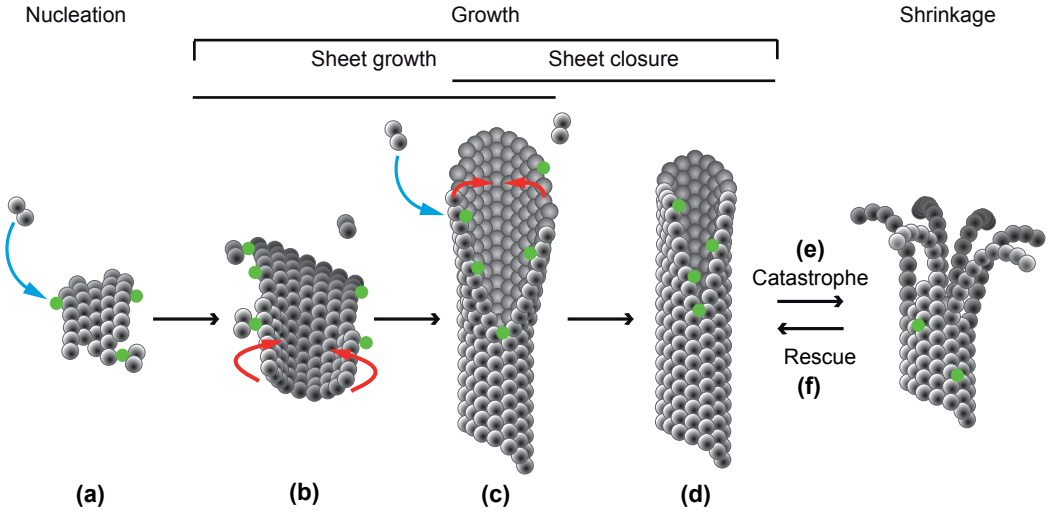

Figure 4. Model for EB1 activity on microtubule assembly and dynamics.
We propose that EB1 (green dots) binds preferentially to the free lateral sites on protofilaments (a), where it facilitates the incorporation of incoming tubulin dimers into the tubulin lattice (blue arrows). This effect stimulates the formation and growth of sheets (b), thereby promoting both nucleation and growth rate. The subsequent increase of the lateral curvature of the sheets leads to their natural closure into tubes (b and c, red arrows). The resulting decrease in sheet length (d) makes microtubules more prone to undergo catastrophe events (e). In addition, during tube closure, EB1 may induce catastrophes by eliminating stressed lattices (see the text for details). At higher concentration, EB1 is no longer restricted to microtubule ends, but also interacts with the microtubule wall. The subsequent reinforcement of tubulin lateral interactions promotes rescues events (f).